

FULL PAPER

Open Access



Slow slip events following the afterslip of the 2002 M_w 7.1 Hualien offshore earthquake, Taiwan

Sean Kuanhsiang Chen^{1*} , Yih-Min Wu^{1,2,3} and Yu-Chang Chan³

Abstract

Geodetic evidence for slow slip recurrence changed by stress perturbations was rare, especially from afterslip following a nearby large earthquake. The first observed slow slip events in the southernmost Ryukyu subduction had occurred in 2005, 2009, and 2015 following the nearby 2002 March 31 M_w 7.1 Hualien offshore earthquake. To investigate whether the M_w 7.1 earthquake had influenced the occurrence times of the slow slip, we calculated the coseismic slip distribution and afterslip distribution using the surface displacements from onshore Global Navigation Satellite System observations. The stress perturbation on the slow-slip regions caused by the coseismic slip was quantified using the Coulomb failure criteria. We also examined the aftershock distribution and the evolution with time to clarify the stress perturbations from the afterslip offshore. Our results show that the primary afterslip distribution may have overlapped the 2009 and 2015 slow-slip patch at the downdip of the earthquake. The coseismic stress perturbation may have influenced the SSEs area directly by a Coulomb stress increase of probably 0.10 MPa. However, the 2005 SSE patch in the updip depths had only a little coseismic slip and afterslip with the Coulomb stress increase of approximately 0.06 MPa. We find that most of the aftershocks had occurred in the 2009 and 2015 slow-slip region that evolved into a typical aftershock sequence at least 2.5 years after the earthquake. The surface geodetic displacements reveal that the afterslip may have lasted longer than 4.5 years after the earthquake. The evidence for the afterslip proves that the 2009 and 2015 slow-slip patch was influenced by the afterslip directly for years. We suggest that the ongoing afterslip may have modulated the coseismic stress perturbation. It may explain the delay of the 2009 slow slip occurrence compared with the recurrence interval between the 2009 and 2015 slow slip events.

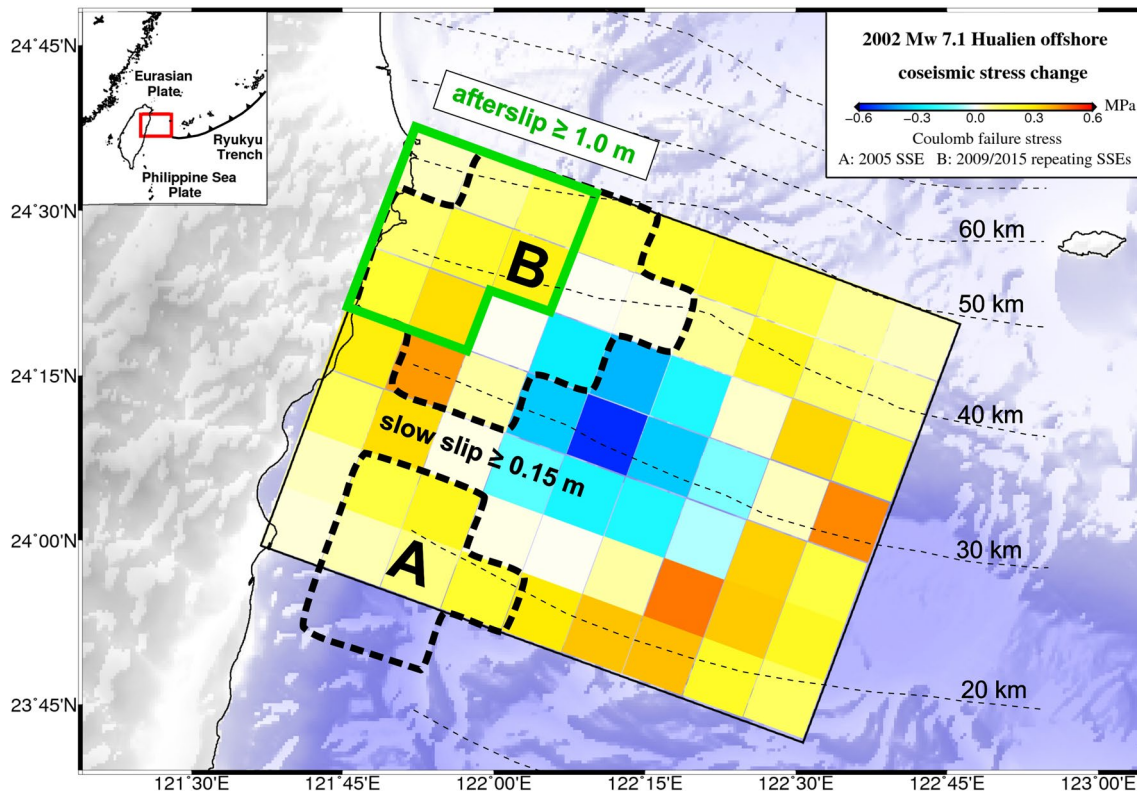
Keywords: Slow slip events, Coseismic slip, Afterslip, Aftershock, Coulomb stress change

*Correspondence: sean80254@gmail.com

¹ Department of Geosciences, National Taiwan University, Taipei 10617, Taiwan

Full list of author information is available at the end of the article

Graphical Abstract



Introduction

Slow slip events (SSEs) in subduction zones usually occur around the seismogenic zone in the updip/down dip/same depths where it is weakly locked (Avouac 2015; Bürgmann 2018; Schwartz and Rokosky 2007). The region where SSEs generate has time-dependent transitional friction probably caused by high-pressure interface fluids (e.g., Behr and Bürgmann 2021; Chen et al. 2018; Saffer and Wallace 2015). The SSEs had recurred with a nearly constant recurrence interval in several subduction zones (e.g., Obara and Kato 2016; Rogers and Dragert 2003; Wallace et al. 2012). Numerical modeling results suggested that the SSEs will recur faster with a shorter recurrence interval after a large seismogenic zone earthquake (Luo and Liu 2019; Matsuzawa et al. 2010, 2013; Segall and Bradley 2012). It may result from stress perturbations on the SSEs region due to seismic wave propagation, coseismic slip, or afterslip from the earthquake (e.g., Luo and Liu 2019; Shibazaki et al. 2019; Wallace et al. 2017). Several pieces of evidence showed that SSE recurs immediately after a large earthquake due to the seismic wave propagation (Cruz-Atienza

et al. 2021; Katakami et al. 2020; Wallace et al. 2017; Wei et al. 2018). The sequence of the Boso SSEs in Japan is the first evidence that the SSEs recurred faster following the coseismic slip and afterslip of the 2011 M_w 9.0 Tohoku earthquake (Hirose et al. 2012; Luo and Liu 2019; Ozawa et al. 2019). Before the Tohoku earthquake, the SSE recurrence interval was approximately 4 to 6 years. After the earthquake, the first SSE occurred in 0.6 years, then SSEs recurred in 2.2 and 4.4 years that nearly recovers to the original recurrence interval (Luo and Liu 2019; Ozawa et al. 2007, 2019). Stress perturbation from the coseismic slip had explained the first SSE that recurred in 0.6 years since the Boso SSEs area experienced a slight coseismic stress increase. Luo and Liu (2019) reproduced the sequence of the shorter recurrence intervals successfully with ongoing stress perturbations from the afterslip. In New Zealand, the Kapiti SSEs recurred approximately 5.0 years (Wallace et al. 2012) before the 2016 M_w 7.8 Kaikōura earthquake. The recurring SSE in 0.5 years after the Kaikōura earthquake was reproduced by the stress perturbations from the afterslip as well (Shibazaki et al. 2019; Wallace et al. 2018). Previous Boso and Kapiti SSEs

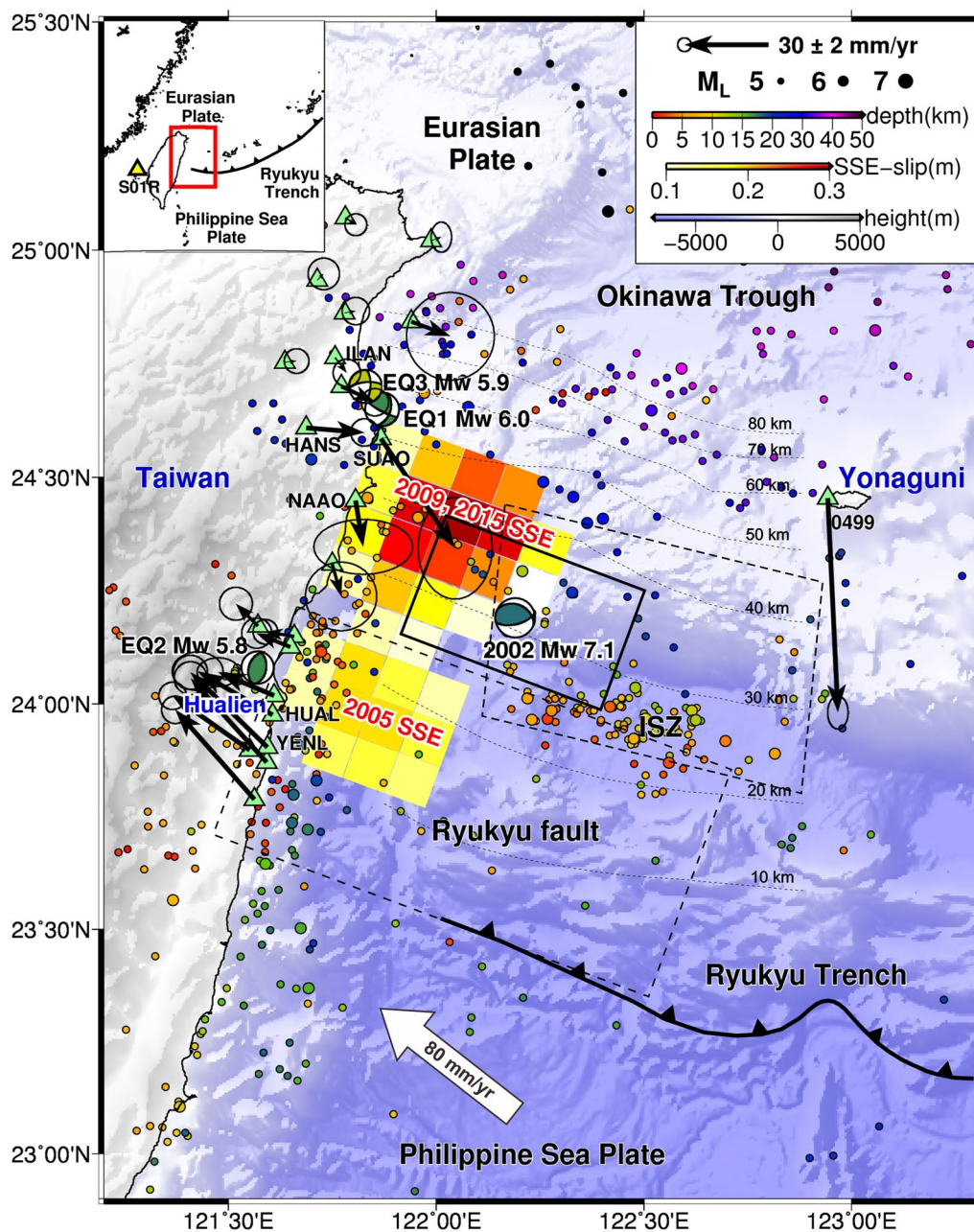


Fig. 1 Overview of SSEs and earthquakes in the southernmost Ryukyu subduction zone from 1991 to 2018. The black rectangle represents the previously studied fault plane of the 2002 March 31 M_w 7.1 Hualien offshore earthquake (Lee et al. 2009). The dotted contours show isodepths of the subducting plate interface from Wu et al. (2009). The cumulative slip of SSEs derived from Chen et al. (2018) and the seismicity derived from the relocated earthquake catalog (Wu et al. 2008) are colored. The dotted rectangles represent the seismogenic structures on the plate interface. ISZ: interplate seismogenic zone (Kao 1998). The horizontal displacements (black arrows) represent the interseismic velocity on the onshore GNSS stations (green triangles) from 2007 to 2016. The horizontal displacements have corrected the effects from the 2002 M_w 7.1 earthquake, three local earthquakes (EQ1 to EQ3 with focal mechanisms), and SSEs. EQ1 to EQ3: the 2002 May 15 M_w 6.0, the 2004 May 1 M_w 5.8, and the 2005 March 7 M_w 5.9 doublet earthquakes. The yellow triangle denotes the reference S01R station

studies have found that the neighboring relation between the SSEs and afterslip regions may have a critical role in the shorter recurrence intervals of SSEs.

Three first-observed SSEs in the southernmost Ryukyu subduction zone in 2005, 2009, and 2015 (Chen et al. 2018) had occurred after the 2002 March 31 M_w 7.1

Hualien offshore earthquake (Fig. 1). Here the Philippine Sea Plate subducts northwestward beneath the Eurasian Plate along the Ryukyu Trench at a rate of approximately 80 mm/year (e.g., Chen et al. 2014, 2017; Hsu et al. 2009). The 2002 M_w 7.1 Hualien offshore earthquake occurred near the depth of the subducting plate interface (Wu et al. 2009) and may have ruptured over an area of 1500 km² (Fig. 1; Lee et al. 2009). The epicenter is located between the western end of the interplate seismogenic zone (ISZ; Kao 1998) and the edge of the SSEs region (Fig. 1). The 2005 SSE may have occurred 40 km southwest of the epicenter in the Ryukyu fault at the downdip depths (Fig. 1; Chen et al. 2018). The Ryukyu fault is a geodetically estimated high coupling region with a slip deficit rate of 86 mm/year from the Ryukyu Trench to the shallow depths of the subducting plate interface (Hsu et al. 2012). The 2009 and 2015 SSEs recurred 20 km northwest of the epicenter in the downdip of the 2005 SSE at the interface depths of nearly 25 to 45 km (Fig. 1a; Chen et al. 2018). The SSE patch is collocated in a high V_p/V_s zone (Huang et al. 2014) and adjacent to a high b -value region (Wu et al. 2018). The 2009 SSE was 7.3 years after the 2002 M_w 7.1 earthquake occurrence, and the 2015 SSE was 6.2 years later than the 2009 SSE (Fig. 2). The time evolution implies the 2009 SSE had been postponed after the 2002 M_w 7.1 earthquake compared with the recurrence interval between the 2009 and 2015 SSEs. As the SSE region is neighboring the 2002 M_w 7.1 earthquake epicenter, the question is what the role of the earthquake was in the occurrence of the 2009 SSE. To this end, we calculated the coseismic slip and afterslip distribution of the 2002 M_w 7.1 earthquake on the plate interface. Then, we estimated the coseismic Coulomb stress change on the SSEs regions and examined the aftershock sequence following the 2002 M_w 7.1 earthquake. Our study indicates that the time delay of the 2009 SSE was very likely resulted from a high overlap between the 2009 SSE and 2002 M_w 7.1 afterslip regions. It provides insights into SSE occurrence linked to afterslip behaviors and how long the influence of afterslip on one SSE patch can sustain.

GNSS data, surface displacements of coseismic slip and afterslip

To calculate the offshore coseismic slip and afterslip distribution for the 2002 M_w 7.1 earthquake, we determined the surface displacements from the nearest onshore

Global Navigation Satellite System (GNSS) observations (Fig. 1). The GNSS data are from the Institute of Earth Science, Academia Sinica of Taiwan, and the Geospatial Information Authority of Japan. However, half of the GNSS stations were operated from one to three years after the 2002 M_w 7.1 earthquake (Additional file 1: Fig. S1). It caused a lack of records of the early afterslip in the GNSS stations, especially those near the epicenter, e.g., the HANS, NAAO, and YENL stations (Fig. 2). We used only 12 stations in northeastern Taiwan (BANC, FIVE, FLNM, HUAL, ILAN, PEPU, S101, SLIN, SUA0, TUNM, YMSM) at the Yonaguni island (0499) in which the records of coseismic slip and afterslip are complete. We used the GNSS data from 2001 to 2016 processed by the Gipsy-X ver 1.3/1.4 software to obtain the time series of daily coordinates under the International Terrestrial Reference Frame (ITRF) 2014 coordinate system. We used the three-component time series to determine the surface displacements of coseismic slip and afterslip following the 2002 M_w 7.1 earthquake. The raw GNSS time series from 2001 to 2016 have recorded several transient signals such as coseismic offsets, postseismic displacements, and SSEs (Fig. 2). The coseismic offsets over the 16-year time series are estimated by the Heaviside function from the 2002 M_w 7.1 earthquake and other local earthquakes, i.e., the 2002 May 15 M_w 6.0, the 2004 May 1 M_w 5.8, and the 2005 March 7 M_w 5.9 doublet events (Figs. 1 and 2). It has been shown the coseismic offset from the 2002 M_w 7.1 earthquake has a maximum of approximately 55 mm on the horizontal components at the SUA0 station (Chen et al. 2004; Fig. 2). The postseismic displacements following the 2002 M_w 7.1 earthquake are modeled with a logarithmic function. Otherwise, there are no significant transient signals regarding the coseismic offsets or postseismic displacements on the 16-year time series. The SSEs detected mainly by the GNSS horizontal components in 2005, 2009, and 2015 are modeled with B^i -spline functions (Riel et al. 2014). The annual and semi-annual movements are modeled by sine and cosine functions. We used the least-squares method to estimate the optimal solution of all the terms on the raw GNSS time series. We demonstrate the examples of three-component time series for the surface displacements of coseismic slip and afterslip following the 2002 M_w 7.1 earthquake in the Additional file 1: Fig. S2. The nearest SUA0 and 0499 stations show the postseismic displacements can be estimated at least to the end

(See figure on next page.)

Fig. 2 GNSS three-component time series and the timings of SSEs, earthquakes, and afterslip. The east and north components are shown by blue and red, respectively. The solid and dotted lines represent the timings of SSEs and the 2002 M_w 7.1 earthquake and EQ1, respectively. The black curves in each time series represent the secular velocity, annual and semi-annual movements, postseismic displacements, and SSEs transient. The location of the GNSS stations and EQ1 to EQ3 are shown in Fig. 1

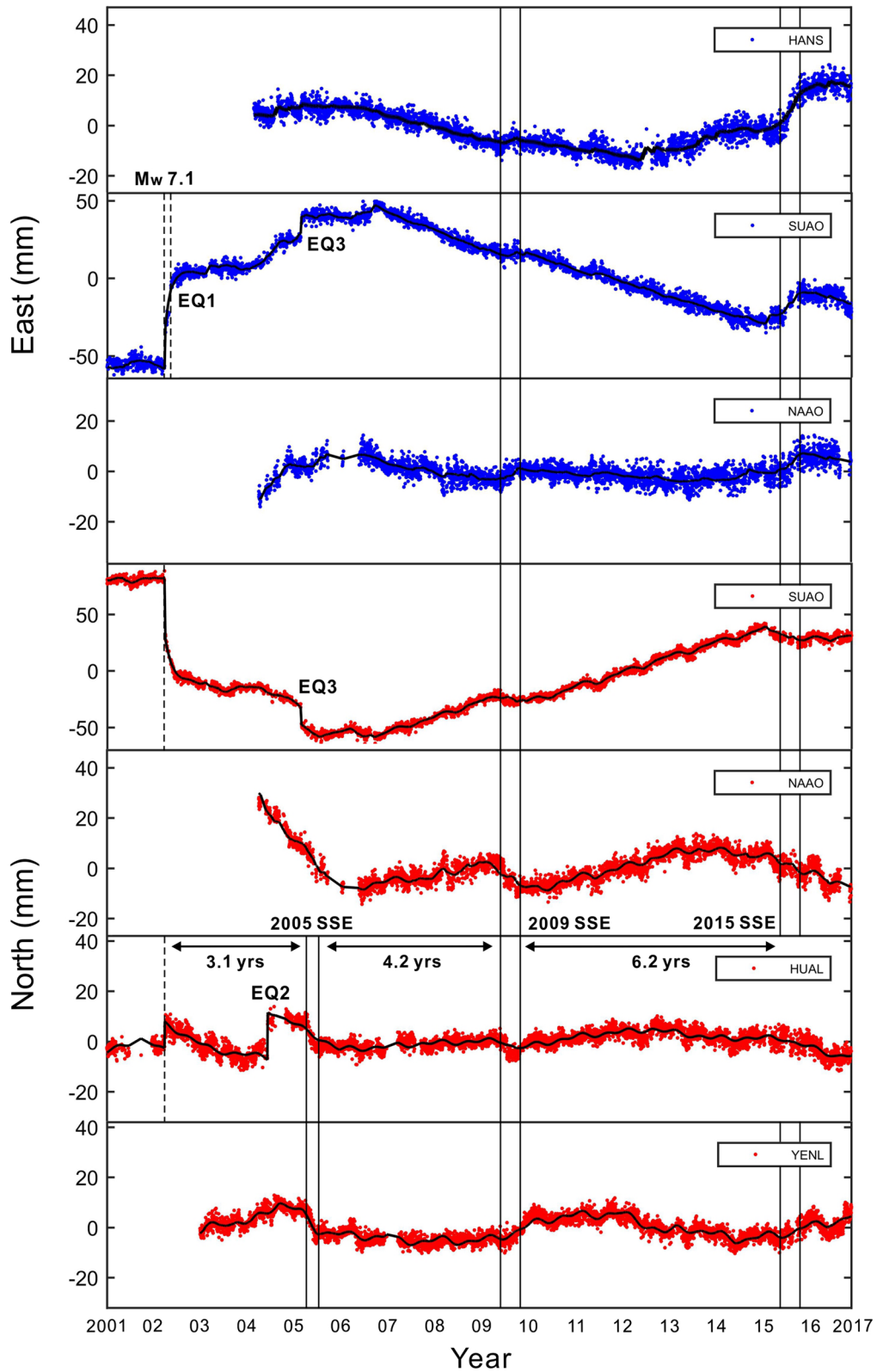


Fig. 2 (See legend on previous page.)

of 2006 in the horizontal components (Additional file 1: Fig. S2). The observed postseismic displacements halted earlier at the end of 2004 in the ILAN and FIVE stations (Additional file 1: Fig. S2), at least 20 km and 50 km northward away from the SUA0 station, respectively. In contrast, the postseismic displacements are small at the PEPU and HUAL stations in the horizontal components (Additional file 1: Fig. S2), 50 km southward away from the SUA0 station. Overall, the horizontal displacement in the observations is coherently much more significant than the vertical displacement (Additional file 1: Fig. S2). This feature that the horizontal movement is more significant agrees with the observed displacements in the westernmost Ryukyu Islands (Nakamura 2009). The uncertainties of the vertical displacements are at least two to five times the horizontal displacements either on the coseismic slip or the afterslip.

Coseismic slip and afterslip inversion and aftershock analysis

The coseismic slip and afterslip of the 2002 M_w 7.1 Hualien offshore earthquake are estimated as homogeneity because the GNSS observations are not close enough to the epicenter area to provide detailed slip heterogeneity (Fig. 1). We assumed both of them have occurred along the subducting plate interface on an interface fault. The coseismic slip and afterslip distribution were reproduced by the slip inversion in an elastic half-space dislocation model (Okada 1992) using the GNSS three-component displacements. The input parameters of the dislocation model are divided into geometric parameters (fault center, strike, dip, length, width, and depth) and slip parameters (strike-slip, dip-slip, and open). We assumed the hypocenter of the 2002 M_w 7.1 earthquake is the fault center, located at the subducting plate interface (Fig. 1). The fault strike (292°), dip (32°), and rake (121°) are from the global centroid moment tensor solution. The fault length and width are assumed to be a dimension of 90×70 km along the subducting plate interface from the depths of 15 to 50 km. The 2002 M_w 7.1 Hualien offshore earthquake is assumed to initiate at the fault center and may have slipped in the rake orientation co-/postseismically. Thus, the peak of the coseismic slip will appear in the fault center, and most of the afterslip will occur in the downdip depths of the coseismic slip region relative to the coseismic slip orientation. We optimized the coseismic slip and afterslip momentums on each subfault plane by the residuals between GNSS three-component displacements and model predictions using the least-squares method. However, the resolution

of offshore slip distribution estimated from observations from the onshore GNSS network would be limited when the area of predicted slip is a distance away from the coastline. Thus, the smoothing of slip momentum was applied during the slip inversion with a Bayesian information criteria (ABIC) (Akaike 1980) to ensure the slip momentum changes continuously on the surrounding subfault plane. We performed a checkerboard test on the interface fault to authenticate that the resolution of coseismic slip and afterslip distribution is valid (Additional file 1: Fig. S3). We applied the resolution matrix (e.g., Yabuki and Matsu'ura 1992; Yokota et al. 2016) as below: $R = (H^T H + \alpha^2 G^T G)^{-1} H^T H$, where H is the static-response-function matrix; α is the hyperparameter of smoothness determined by the ABIC; G is the spatial smoothness matrix. T denotes the transposed matrix. We generated synthetic data for the checkerboard-like slip distribution with two standard deviation errors of 1.0 m for the onshore GNSS coseismic data. The synthetic data and their standard deviation error are generated and determined by a bootstrapped method. The optimal size of every inversion grid on the entire subfault plane mainly depends on the anomaly of slip momentum that the nearby GNSS data can resolve until reliable slip patterns are reproduced. We demonstrated an example of the checkerboard-like slip distribution with the reproduced slip in Additional file 1: Fig. S3. The reproduced slip distribution in the checkerboard test shows an acceptable resolution except for the slip area at the southeast updip corner of the subfault planes (Additional file 1: Fig. S3b and c). The resolution value as diagonal elements of the resolution matrix shows a poor resolution (< 0.15) of the local reproduced slip. Thus, the slip pattern (both the coseismic slip and afterslip) at the southeast updip corner of the subfault planes is not discussed. Since aftershocks accompanied afterslip primarily (e.g., Hsu et al. 2006; Peng and Zhao 2009), it can provide additional evidence for the afterslip offshore. For example, aftershocks show the locations where the crustal stresses are relieved during the evolution of the afterslip. To further validate the afterslip process, we analyzed the aftershock distribution on the interface fault region and the aftershock evolution with time using a relocated earthquake catalog (Wu et al. 2008). It provides an improved location quality derived from the standard earthquake catalog from the Central Weather Bureau of Taiwan. We analyzed the relocated earthquakes only with local magnitudes (M_L) ≥ 2.0 and depths ≤ 40 km in the interface fault region. We also examined the aftershock evolution in the two SSE regions

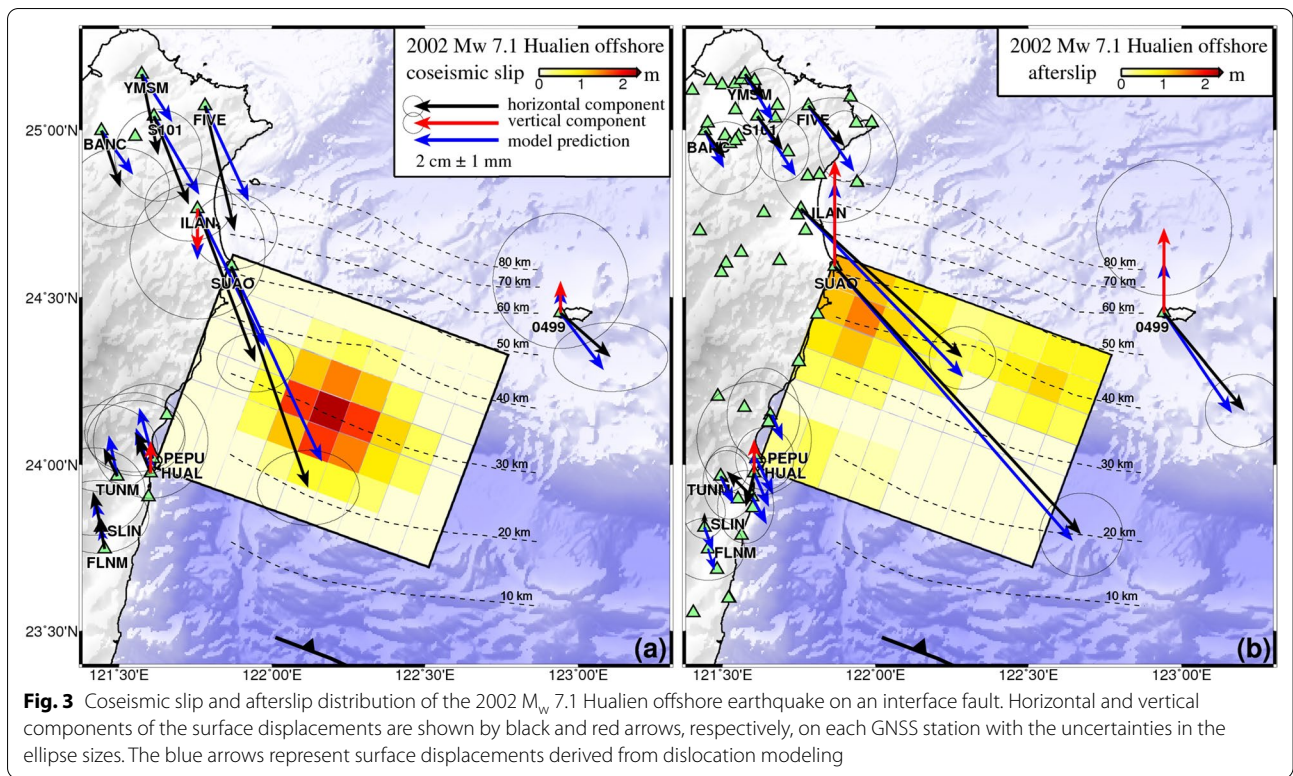


Fig. 3 Coseismic slip and afterslip distribution of the 2022 M_w 7.1 Hualien offshore earthquake on an interface fault. Horizontal and vertical components of the surface displacements are shown by black and red arrows, respectively, on each GNSS station with the uncertainties in the ellipse sizes. The blue arrows represent surface displacements derived from dislocation modeling

to clarify the possible relation between afterslip and SSE occurrence.

Coulomb stress change caused by the coseismic slip

We employed the Coulomb failure criteria (e.g., King et al. 1994; Stein 1999; Toda et al. 2011) to quantify stress perturbation on the SSEs regions caused by the coseismic slip of the 2022 M_w 7.1 Hualien offshore earthquake. The Coulomb stress change $\Delta\sigma_c$ is $\Delta\sigma_c = \Delta\tau - \mu\Delta\sigma_n$, where $\Delta\tau$ is shear stress change, $\Delta\sigma_n$ is normal stress change, and μ is the effective friction coefficient. $\Delta\sigma_c$, $\Delta\tau$, and $\Delta\sigma_n$ are estimated from the 3D strain field on the specified receiver faults derived from the coseismic slip on the subducting plate interface (the source fault). The coseismic slip is multiplied by the elastic stiffness to obtain the 3D strain field and $\Delta\sigma_c$. Poisson’s ratio (PR) and Young’s modulus (E) are used as 0.25 and 80 GPa, respectively. For the interface slip of the 2022 M_w 7.1 earthquake at nearly 20 to 30 km, we assumed the friction coefficient as 0.3 for a subducting oceanic plate interface (Ikari et al. 2018; Kaneki and Hirono 2019; Namiki et al. 2014). Thus, the shear modulus of G is $G = E/[2(1 + PR)] = 30$ GPa. We designed a receiver fault that each subfault plane has specified strike, dip, and rake, to combine them into the

source fault model to make the coseismic static stresses convey validly. The receiver faults begin from all patches outside of the primary coseismic slip region, and thus the Coulomb stress change is positive on the receiver faults. In addition, the Coulomb failure is estimated from the coseismic slip theoretically for the stress drop: $\Delta\sigma \approx GD/\sqrt{A}$, where D is the average slip on the patch and A is the patch area. Since the SSEs were neighboring the epicenter of the 2022 M_w 7.1 Hualien offshore earthquake, the SSEs areas may have been experienced directly by the coseismic stress perturbation. In other words, the increase and decrease in the spatial Coulomb stresses may appear in the SSEs areas simultaneously, different from observations in the Boso and Kapiti SSEs areas. For simplicity, we calculated the mean Coulomb stress change on the two SSE regions only where the cumulative peak slip appeared. Here the cumulative peak slip is defined as the cumulative slip exceeding 0.15 m on the subducting plate interface. The simplicity helps us examine the overall spatial relation among the stress perturbations, afterslip distribution, and SSE occurrence. We determined the uncertainty of the mean Coulomb stress change from the one standard deviation of the stress changes on each subfault patch.

Coseismic slip, afterslip/aftershocks, and Coulomb stress change following the 2002 M_w 7.1 Hualien offshore earthquake

We demonstrated the coseismic slip and afterslip distribution of the 2002 M_w 7.1 Hualien offshore earthquake in the subfault planes of 100 km^2 , which is valid for the interface slip offshore (Additional file 1: Fig. S3). Our inversion results show that both of them predicted by the dislocation modeling are mainly within the uncertainties of the observed horizontal displacements (Fig. 3). The primary coseismic slip distribution is at the interface depths of 25 to 35 km with a maximum slip of 2.3 m (Fig. 3a). The coseismic slip distribution changes continuously in the subfault planes away from the maximum-slip area

(Fig. 3a). The coseismic slip decreases to less than 0.2 m in the subfault planes at least 25 km away from the maximum coseismic slip area. We observed the primary afterslip distribution depth is 35 to 50 km at the northwest downdip of the coseismic slip region (Fig. 3b). The local afterslip shows a maximum afterslip of 1.5 m dominated by the SUA0 and ILAN stations near the northwestern downdip limit of the fault plane (Fig. 3b). It is no doubt that the two have the largest horizontal displacements from the overall observations around the epicenter of the 2002 M_w 7.1 earthquake during the afterslip (Fig. 3b). The secondary afterslip of 1.0 m may appear in the northeast downdip of the coseismic slip region related to the south-eastward displacements of the 0499 station. However, we

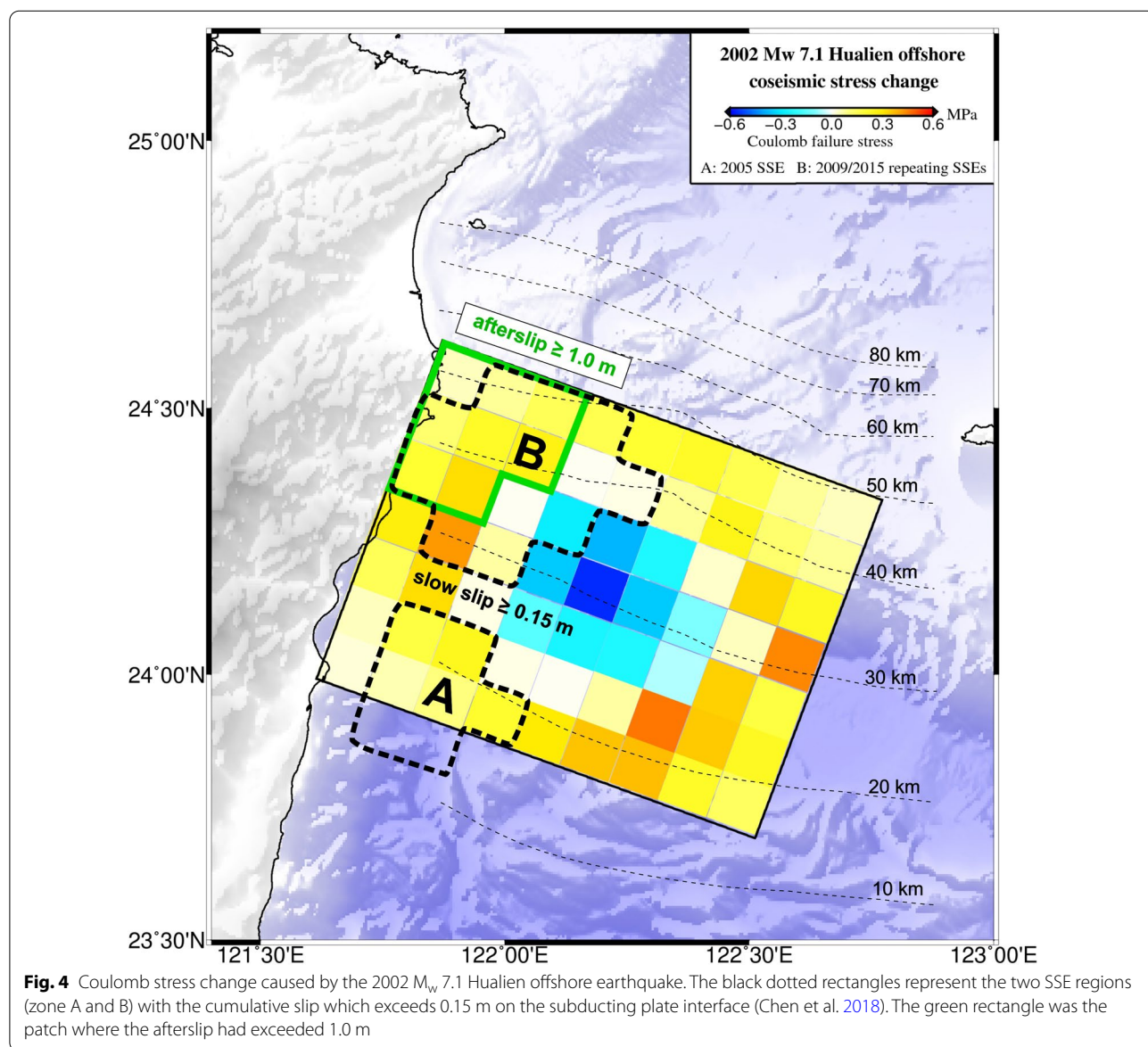
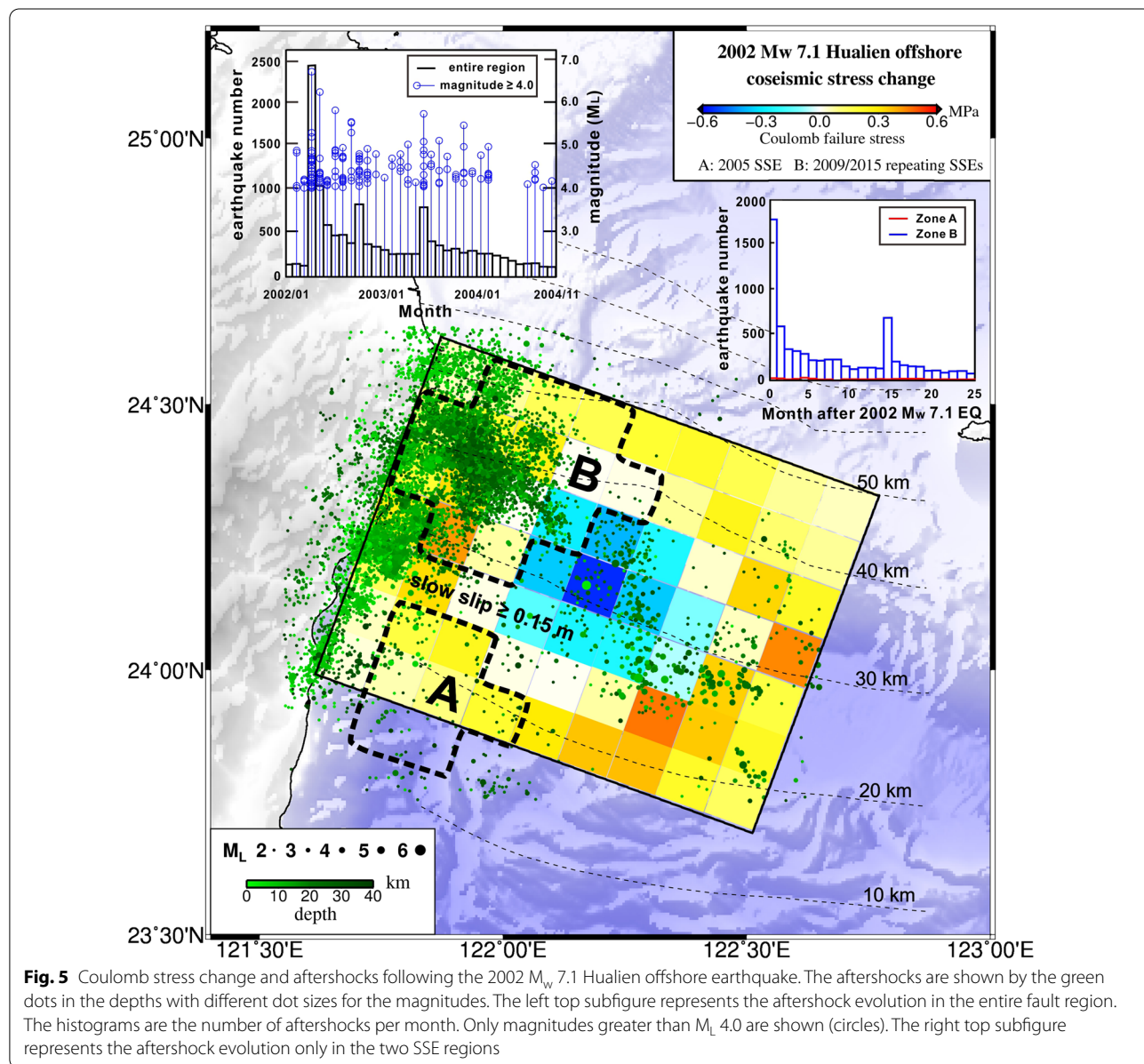


Fig. 4 Coulomb stress change caused by the 2002 M_w 7.1 Hualien offshore earthquake. The black dotted rectangles represent the two SSE regions (zone A and B) with the cumulative slip which exceeds 0.15 m on the subducting plate interface (Chen et al. 2018). The green rectangle was the patch where the afterslip had exceeded 1.0 m

observed very little afterslip in the updip of the coseismic maximum-slip area. A few afterslip of 0.2 to 0.4 m may occur near the southwest updip constrained by a group of GNSS stations with a few horizontal displacements (Fig. 3b). Figure 4 shows the Coulomb stress change on the two SSE regions caused by the coseismic slip of the 2002 M_w 7.1 Hualien offshore earthquake. The stress drop in the maximum coseismic slip area is estimated at nearly 0.55 MPa and decreases continuously along the fault dip and strike directions. The Coulomb stress increase may have occurred around the edge of the stress drop region with the maximum increase of 0.45 MPa (Fig. 4). The Coulomb stress increase also decreases

continuously further away from the stress drop region and becomes nearly no increase in the edge of the sub-fault planes. Our results show that the 2005 SSE region and the 2009/2015 SSEs region are both influenced by the coseismic stress perturbation and overlapped with the region of Coulomb stress increase (Fig. 4). The mean Coulomb stress increase is weak in the peak slip region of the 2005 SSE (so-called zone A afterward), approximately 0.06 ± 0.02 MPa (Fig. 4). Such stress increase is probably 0.10 ± 0.05 MPa in the peak slip region of the 2009 and 2015 SSEs (zone B). Since zone B is much closer to the 2002 M_w 7.1 earthquake epicenter, it may have been influenced by the coseismic stress perturbations more



directly. The uncertainty of the mean Coulomb stress change is inevitable. We find that zone B was experienced by the afterslip primarily, i.e., the afterslip exceeds 1.0 m (Fig. 4). Figure 5 shows the aftershock distribution on the interface fault around the epicenter of the 2002 M_w 7.1 earthquake. We find that most of the aftershocks had occurred in the northwest downdip depths of the stress drop region, which is the primary afterslip distribution depths (Fig. 5). The aftershocks are much fewer in the updip depths of the stress drop region, especially in zone A where the afterslip is very little (Fig. 5). The observations support the reliability of the estimated afterslip distribution as we know afterslip is accompanied by aftershocks primarily (e.g., Hsu et al. 2006; Peng and Zhao 2009). Figure 5 also shows the aftershock evolution with time. Overall, the number of aftershocks reduces rapidly in the first few months after the earthquake occurrence, 2002 March 31 (Fig. 5 left top). Then, the reduction of aftershocks changes into a slow rate till the end of 2004, to the level of the monthly earthquake number before the earthquake occurrence (Fig. 5 left top). We also find the number of aftershocks in zone B reduces exponentially with time at least 20 months after the M_w 7.1 earthquake (Fig. 5 right top). However, the number of aftershocks in zone A does not typically show an aftershock sequence as an exponential decay in the number of aftershocks with time. The evidence of the aftershock evolution indicated that zone B was influenced by the afterslip primarily.

Discussion

SSEs recurring on the same patch represent a repeated stress relief during crustal stress accumulation on the subducting plate interface. The stress perturbations from afterslip had explained the shorter recurrence interval of SSEs after a nearby large earthquake. This case is valid if the afterslip had occurred outside the SSE patch and evolved into a decelerated stress rate with time as observed (e.g., Hu et al. 2016; Wang et al. 2012). The evidence of the sequence of the Boso SSE (e.g., Luo and Liu 2019) and creep events in the Salton Trough (e.g., Wei et al. 2015) have validated the time-dependent stress perturbations on the shorter recurrence interval. However, we observed a likely longer recurrence interval of SSEs after the 2002 M_w 7.1 earthquake in the southernmost Ryukyu subduction zone. It has been shown that SSEs can be triggered immediately by the coseismic stress perturbations caused by the seismic wave propagation at 0.065 to 0.2 MPa on the surroundings of a seismogenic zone or remotely (e.g., Cruz-Atienza et al. 2021; Katakami et al. 2020; Wallace et al. 2017; Wei

et al. 2018). The triggering stress threshold on the SSE patch may vary with the stressed and frictional conditions on the patch interface. Stress perturbation caused by the coseismic slip from the 2002 M_w 7.1 earthquake on zone B, where the 2009 and 2015 SSEs have recurred, was approximately from 0.05 to 0.15 MPa. This stress value may have exceeded the lower limit of the previously observed triggering stress threshold on the SSE patch. Here, we only consider coseismic stress perturbation caused by the coseismic slip and do not discuss the effect of seismic wave propagation. If we consider both stress perturbations on the SSE patch, the summed stress value would be more significant than currently estimated. The timing that SSEs recurred on the same patch also represents the transitional friction occurring on the fault interface from the state of velocity weakening to velocity strengthening (e.g., Bürgmann 2018; Ikari et al. 2013; Saffer and Wallace, 2015). In most periods without SSE activity, the frictional properties on the SSE patch could be velocity weakening to restrain the occurrence of SSE. If so, the 2009 SSE did not immediately occur on zone B after the 2002 M_w 7.1 earthquake may result from the temporal variations of interplate friction, as inferred in this subduction zone from onshore GNSS observations (Chen et al. 2018). However, the SSE that occurred in zone B in 2009 is about 7.3 years later than the 2002 M_w 7.1 earthquake, which is a long delay after the coseismic stress perturbations. We suggest that a high overlap between the SSE patch and the primary afterslip distribution may have played a critical role in the delay of the SSE occurrence. The evidence of GNSS surface displacements revealed that the afterslip may have lasted till the end of 2006 (Fig. 2). Note that the aftershocks in zone B seem to pause earlier than the afterslip at the end of 2004 (Fig. 5). Considering both evidence together, it implies that the Coulomb stress increase in zone B may have been relieved by the ongoing afterslip in the following 2.5 to 4.5 years. Afterward, the interface friction on zone B changed into the state of velocity weakening with high frictional from 2007 to the middle of 2009 (stress accumulation), then the SSE occurred. The stress modulation on zone B from the afterslip between 2002 April and 2007 might postpone the 2009 SSE occurrence. Since the afterslip no longer affected zone B afterward, we assumed the recurrence interval between the 2009 and 2015 SSEs as the typical SSE cycle. It is worthwhile to model the stress modulation of afterslip on the SSE patch and quantify the time delay of SSE. In contrast, the afterslip was very little in zone A which makes the stress modulation of the afterslip unreasonable to explain the delay of 2005 SSE

occurrence. The coseismic stress perturbation on zone A caused by the coseismic slip of the 2002 M_w 7.1 earthquake was approximately from 0.04 to 0.08 MPa, which may have approached the aforementioned triggering stress threshold of SSE. Since only one SSE occurred in zone A in 2005 and this region is overlapped by the highly coupled Ryukyu fault, the occurrence of SSE in 3.1 years after the 2002 M_w 7.1 earthquake may be explained by a delayed triggering of coseismic stress perturbation. Some studies have shown that SSEs coexist at the edge of a locked fault region where transitional friction may occur (e.g., Dixon et al. 2014; Ito et al. 2013; Mallick et al. 2021). The episode of transitional friction with a small-scale heterogeneity could be a reason for the SSE generation, as observed in the Japan Trench and Costa Rica subduction zones (e.g., Dixon et al. 2014; Ito et al. 2013). Here, we cannot rule out the possibility that the 2005 and 2009 SSEs occurrences are independent of the stress perturbations from coseismic slip and afterslip following the 2002 M_w 7.1 earthquake. A sequence of SSEs in Costa Rica had shown that the recurrence interval did not change after the 2012 M_w 7.6 Nicoya earthquake (Voss et al. 2017; Xie et al. 2020). Continuous monitoring of future SSEs in the southernmost Ryukyu subduction zone will clarify the recurrence interval of SSEs linked to the afterslip.

Conclusions

This study investigated coseismic Coulomb stress change, afterslip behaviors, and occurrence of SSE in the SSE area where afterslip had accompanied. We quantified Coulomb stress change on two SSE regions in the southernmost Ryukyu subduction zone caused by the neighboring 2002 M_w 7.1 Hualien offshore earthquake. The Coulomb stress increase is approximately 0.06 MPa in the 2005 SSE patch at the shallower depths of the subducting plate interface. The coseismic stress perturbation may have approached the triggering stress threshold of SSE as observed in the Nankai, Hikurangi, and Guerrero subduction zones. We found that this SSE region has only very little afterslip and aftershocks following the 2002 M_w 7.1 earthquake, especially, SSE no longer recurs in this region after 2005. The high interface friction on the SSE patch may explain the SSE as a delayed triggering of the coseismic stress perturbation. We also found that the 2009 and 2015 SSEs patch is primarily experienced by the afterslip together with long-lived aftershocks. The number of aftershocks in this SSEs region evolved into a typical aftershock sequence after the 2002 M_w 7.1 earthquake till the end of 2004. However, GNSS surface displacements have shown that the afterslip lasted much longer to the end of 2006. The evidence of the evolution

of afterslip indicates that the afterslip may have relieved the Coulomb stress increase on the SSE patch in the following 2.5 to 4.5 years. Afterward, the patch interface changed into high frictional to accumulate the crustal stresses. The stress modulation of afterslip might explain the delay of 2009 SSE occurrence since coseismic stress perturbation on the SSE patch may have reached the previously observed triggering stress threshold. Our study can provide more insights into the linkage from stress perturbations of afterslip to SSE occurrence or even recurrence.

Abbreviations

SSEs: Slow slip events; ISZ: Interplate seismogenic zone; GNSS: Global Navigation Satellite System; EQ: Earthquake; M_w : Moment magnitude; M_L : Local magnitude; GPa: Gigapascal; MPa: Megapascal; mm: Millimeter; mm/yr: Millimeter per year; m: Meter; km^2 : Square kilometer; V_p/V_s : The ratio of seismic compressional and shear-wave velocities; ITRF: International Terrestrial Reference Frame; ABIC: A Bayesian information criteria.

Supplementary Information

The online version contains supplementary material available at <https://doi.org/10.1186/s40623-022-01629-y>.

Additional file 1: Figure S1. Development of the onshore GNSS stations in the northeastern Taiwan region. **a.** Before the 2002 March 31 M_w 7.1 Hualien offshore earthquake. **b.** Before the 2005 SSE. **c.** After the 2005 SSE. The named stations are the same as Fig. 3 for the coseismic slip and afterslip inversion. **Figure S2.** GNSS three-component time series of coseismic offsets and postseismic displacements following earthquakes. The vertical line denotes the timing of the 2002 M_w 7.1 Hualien offshore earthquake. The black curves in each time series represent the secular velocity, annual and semi-annual movements, coseismic offsets, and postseismic displacements. The dotted lines denote the detrended GNSS velocities before the earthquake. EQ1 to EQ3 are the local earthquakes marked in Fig. 1. The location of the six GNSS stations is labeled in Fig. 3. **Figure S3.** Checkerboard test for the coseismic slip distribution of the 2002 M_w 7.1 Hualien offshore earthquake on the subducting plate interface. The synthetic input slip is generated with two standard deviation errors of 1.0 m. The onshore GNSS stations are the same as shown in Fig. 3.

Acknowledgements

We appreciate the Editor and the two anonymous reviewers for constructive comments to improve the manuscript. We acknowledge the Institute of Earth Sciences, Academia Sinica, Taiwan, providing the GNSS data.

Author contributions

SK Chen conceptualized the study and analyzed the data. SK Chen, YM Wu, and YC Chan wrote the manuscript. All authors read and approved the final manuscript.

Funding

This study was funded by the Ministry of Science and Technology (MOST) in Taiwan under grant number 109-2116-M-002-030-MY3.

Availability of data and materials

The GNSS data are available at <http://gdbweb.earth.sinica.edu.tw/>. The Coulomb stress calculations were performed using Coulomb 3 software, available from <https://www.usgs.gov/node/279387>.

Declarations

Ethics approval and consent to participate

Not applicable.

Consent for publication

Not applicable.

Competing interests

The authors declare that they have no competing interests.

Author details

¹Department of Geosciences, National Taiwan University, Taipei 10617, Taiwan.

²Research Center for Future Earth, National Taiwan University, Taipei 10617, Taiwan. ³Institute of Earth Sciences, Academia Sinica, Taipei 11529, Taiwan.

Received: 19 January 2022 Accepted: 11 April 2022

Published online: 26 April 2022

References

- Akaike H (1980) Likelihood and the Bayes procedure. In: Bernardo JM, De Groot MH, Lindley DV, Smith AFM (eds) Bayesian statistics. University Press, Valencia, pp 143–166
- Avouac JP (2015) From geodetic imaging of seismic and aseismic fault slip to dynamic modeling of the seismic cycle. *Ann Rev Earth Planet Sci* 43:233–271. <https://doi.org/10.1146/annurev-earth-060614-105302>
- Behr WM, Burgmann R (2021) What's down there? The structures, materials and environment of deep-seated slow slip and tremor. *Philos Trans R Soc* 379:20200218. <https://doi.org/10.1098/rsta.2020.0218>
- Bürgmann R (2018) The geophysics, geology and mechanics of slow fault slip. *Earth Planet Sci Lett* 495:112–134. <https://doi.org/10.1016/j.epsl.2018.04.062>
- Chen HY, Kuo LC, Yu SB (2004) Coseismic movement and seismic ground motion associated with the 31 March 2002 off Hualien, Taiwan, Earthquake. *Terr Atmos Ocean Sci* 15:683–695. [https://doi.org/10.3319/TAO.2004.15.4.683\(T\)](https://doi.org/10.3319/TAO.2004.15.4.683(T))
- Chen SK, Chan YC, Hu JC, Kuo LC (2014) Current crustal deformation at the junction of collision to subduction around the Hualien area. *Taiwan Tectonophysics* 617:58–78. <https://doi.org/10.1016/j.tecto.2014.01.014>
- Chen SK, Wu YM, Hsu YJ, Chan YC (2017) Current crustal deformation of the Taiwan orogen reassessed by cGPS strain-rate estimation and focal mechanism stress inversion. *Geophys J Int* 210:228–239. <https://doi.org/10.1093/gji/ggx165>
- Chen SK, Wu YM, Chan YC (2018) Episodic slow slip events and overlying plate seismicity at the southernmost Ryukyu Trench. *Geophys Res Lett* 45:10369–10377. <https://doi.org/10.1029/2018GL079740>
- Cruz-Atienza VM, Tago J, Villafuerte C, Wei M, Garza-Giron R, Dominguez LA et al (2021) Short-term interaction between silent and devastating earthquakes in Mexico. *Nat Comm* 12:2171. <https://doi.org/10.1038/s41467-021-22326-6>
- Dixon TH, Jiang Y, Malservisi R, McCaffrey R, Voss N, Protti M, Gonzalez V (2014) Earthquake and tsunami forecasts: relation of slow slip events to subsequent earthquake rupture. *Proc Natl Acad Sci* 111:17039–17044. <https://doi.org/10.1073/pnas.1412299111>
- Hirose H, Kimura H, Bogdan Enescu B, Aoi S (2012) Recurrent slow slip event likely hastened by the 2011 Tohoku earthquake. *Proc Natl Acad Sci* 109:15157–15161. <https://doi.org/10.1073/pnas.1202709109>
- Hsu YJ, Simons M, Avouac JP, Galetzka J, Sieh K, Chlieh M, Natawidjaja D, Prawirodirdjo L, Bock Y (2006) Frictional afterslip following the 2005 Nias-Simeulue earthquake, Sumatra. *Science* 312:1921–1926. <https://doi.org/10.1126/science.1126960>
- Hsu YJ, Yu SB, Simons M, Kuo LC, Chen HY (2009) Interseismic crustal deformation in the Taiwan plate boundary zone revealed by GPS observations, seismicity, and earthquake focal mechanisms. *Tectonophysics* 479:4–18. <https://doi.org/10.1016/j.tecto.2008.11.016>
- Hsu YJ, Ando M, Yu SB, Simons M (2012) The potential for a great earthquake along the southernmost Ryukyu subduction zone. *Geophys Res Lett* 39:L14302. <https://doi.org/10.1029/2012GL052764>
- Hu Y, Bürgmann R, Uchida N, Banerjee P, Freymueller JT (2016) Stress-driven relaxation of heterogeneous upper mantle and time-dependent afterslip following the 2011 Tohoku earthquake. *J Geophys Res* 121:385–411. <https://doi.org/10.1002/2015JB012508>
- Huang HH, Wu YM, Song XD, Chang CH, Lee SC, Chang TM, Hsieh HH (2014) Joint V_p and V_s tomography of Taiwan: implications for subduction-collision orogeny. *Earth Planet Sci Lett* 392:177–191. <https://doi.org/10.1016/j.epsl.2014.02.026>
- Ikari MJ, Marone C, Saffer DM, Kopf AJ (2013) Slip weakening as a mechanism for slow earthquakes. *Nat Geosci* 6:468–472. <https://doi.org/10.1038/ngeo1818>
- Ikari MJ, Kopf AJ, Hüpers A, Vogt C (2018) Lithologic control of frictional strength variations in subduction zone sediment inputs. *Geosphere* 14:604–625. <https://doi.org/10.1130/GES01546.1>
- Ito Y, Hino R, Kido M, Fujimoto H, Osada Y, Inazu D et al (2013) Episodic slow slip events in the Japan subduction zone before the 2011 Tohoku-Oki earthquake. *Tectonophysics* 600:14–26. <https://doi.org/10.1016/j.tecto.2012.08.022>
- Kaneki S, Hirono T (2019) Diagenetic and shear-induced transitions of frictional strength of carbon-bearing faults and their implications for earthquake rupture dynamics in subduction zones. *Sci Rep* 9:7884. <https://doi.org/10.1038/s41598-019-44307-y>
- Kao H (1998) Can great earthquakes occur in the southernmost Ryukyu arc-Taiwan region? *Terr Atmos Ocean Sci* 9:487–508. <https://doi.org/10.3319/TAO.1998.9.3.487>
- Katakami S, Kaneko Y, Ito Y, Araki E (2020) Stress sensitivity of instantaneous dynamic triggering of shallow slow slip events. *J Geophys Res*. <https://doi.org/10.1029/2019JB019178>
- King GCP, Stein RS, Lin J (1994) Static stress changes and the triggering of earthquakes. *Bull Seis Soc Am* 84:935–953. <https://doi.org/10.1785/BSSAO840030935>
- Lee SJ, Komatitsch D, Huang BS, Tromp J (2009) Effects of topography on seismic-wave propagation: an example from Northern Taiwan. *Bull Seis Soc Am* 99:314–325. <https://doi.org/10.1785/0120080020>
- Luo Y, Liu Z (2019) Slow-slip recurrent pattern changes: perturbation responding and possible scenarios of precursor toward a megathrust earthquake. *Geochem Geophys Geosys* 20:852–871. <https://doi.org/10.1029/2018GC008021>
- Mallick R, Meltzner AJ, Tsang LLH, Lindsey EO, Feng L, Hill EM (2021) Long-lived shallow slow-slip events on the Sunda megathrust. *Nat Geosci* 14:327–333. <https://doi.org/10.1038/s41561-021-00727-y>
- Matsuzawa T, Hirose H, Shibazaki B, Obara K (2010) Modeling short-and long-term slow slip events in the seismic cycles of large subduction earthquakes. *J Geophys Res* 115:B12301. <https://doi.org/10.1029/2010JB007566>
- Matsuzawa T, Shibazaki B, Obara K, Hirose H (2013) Comprehensive model of short-and long-term slow slip events in the Shikoku region of Japan, incorporating a realistic plate configuration. *Geophys Res Lett* 40:5125–5130. <https://doi.org/10.1002/grl.51006>
- Nakamura M (2009) Aseismic crustal movement in southern Ryukyu Trench, southwest Japan. *Geophys Res Lett* 36:L20312. <https://doi.org/10.1029/2009GL040357>
- Namiki Y, Tsutsumi A, Ujiie K, Kameda J (2014) Frictional properties of sediments entering the Costa Rica subduction zone offshore the Osa Peninsula: implications for fault slip in shallow subduction zones. *Earth Planets Space* 66:72. <https://doi.org/10.1186/1880-5981-66-72>
- Obara K, Kato A (2016) Connecting slow earthquakes to huge earthquakes. *Science* 353:253–257. <https://doi.org/10.1126/science.aaf1512>
- Okada Y (1992) Internal deformation due to shear and tensile faults in a half-space. *Bull Seis Soc Am* 82:1018–1040
- Ozawa S, Suito H, Tobita M (2007) Occurrence of quasi-periodic slow slip off the east coast of the Boso peninsula, central Japan. *Earth Planets Space* 59:1241–1245. <https://doi.org/10.1186/BF03352072>
- Ozawa S, Yarai H, Kobayashi T (2019) Recovery of the recurrence interval of Boso slow slip events in Japan. *Earth Planets Space* 71:78. <https://doi.org/10.1186/s40623-019-1058-y>
- Peng Z, Zhao P (2009) Migration of early aftershocks following the 2004 Parkfield earthquake. *Nat Geosci* 2:877–881. <https://doi.org/10.1038/NNGEO697>

- Riel B, Simons M, Agram P, Zhan Z (2014) Detecting transient signals in geodetic time series using sparse estimation techniques. *J Geophys Res* 119:5140–5160. <https://doi.org/10.1002/2014JB011077>
- Rogers G, Dragert H (2003) Episodic tremor and slip on the Cascadia subduction zone: the chatter of silent slip. *Science* 330:1942–1943. <https://doi.org/10.1126/science.1084783>
- Saffer DM, Wallace LM (2015) The frictional, hydrologic, metamorphic and thermal habitat of shallow slow earthquakes. *Nat Geosci* 8:594–600. <https://doi.org/10.1038/ngeo2490>
- Schwartz SY, Rokosky JM (2007) Slow slip events and seismic tremor at circum-Pacific subduction zones. *Rev Geophys* 45:RG3004. <https://doi.org/10.1029/2006RG000208>
- Segall P, Bradley AM (2012) Slow-slip evolves into megathrust earthquakes in 2D numerical simulations. *Geophys Res Lett* 39:L18308. <https://doi.org/10.1029/2012GL052811>
- Shibazaki B, Wallace LM, Kaneko Y, Hamling I, Ito Y, Matsuzawa T (2019) Three-dimensional modeling of spontaneous and triggered slow-slip events at the Hikurangi subduction zone, New Zealand. *J Geophys Res* 124:13250–13268. <https://doi.org/10.1029/2019JB018190>
- Stein RS (1999) The role of stress transfer in earthquake occurrence. *Nature* 402:605–609. <https://doi.org/10.1038/45144>
- Toda S, Stein RS, Sevilgen V, Lin J (2011) Coulomb 3.3 Graphic-rich deformation and stress-change software for earthquake, tectonic, and volcano research and teaching—user guide. In: U.S. Geological Survey Open-File Report 2011–1060, p. 63. <https://doi.org/10.3133/ofr20111060>
- Voss N, Malservisi R, Dixon TH, Protti M (2017) Slow slip events in the early part of the earthquake cycle. *J Geophys Res* 122:6773–6786. <https://doi.org/10.1002/2016JB013741>
- Wallace LM, Barnes P, Beavan J, Van Dissen R, Litchfield N, Mountjoy J et al (2012) The kinematics of a transition from subduction to strike-slip: an example from the central New Zealand plate boundary. *J Geophys Res* 117:B02405. <https://doi.org/10.1029/2011JB008640>
- Wallace LM, Kaneko Y, Hreinsdóttir S, Hamling I, Peng Z, Bartlow N, D'Anastasio E, Fry B (2017) Large-scale dynamic triggering of shallow slow slip enhanced by overlying sedimentary wedge. *Nat Geosci* 10:765–770. <https://doi.org/10.1038/ngeo3021>
- Wallace LM, Hreinsdóttir S, Ellis S, Hamling I, D'Anastasio E, Denys P (2018) Triggered slow slip and afterslip on the southern Hikurangi subduction zone following the Kaikōura earthquake. *Geophys Res Lett* 45:4710–4718. <https://doi.org/10.1002/2018GL077385>
- Wang K, Hu Y, He J (2012) Deformation cycles of subduction earthquakes in a viscoelastic Earth. *Nature* 484:327–332. <https://doi.org/10.1038/nature11032>
- Wei M, Liu Y, Kaneko Y, McGuire JJ, Bilham R (2015) Dynamic triggering of creep events in the Salton Trough, Southern California by regional $M \geq 5.4$ earthquakes constrained by geodetic observations and numerical simulations. *Earth Planet Sci Lett* 532:115970. <https://doi.org/10.1016/j.epsl.2019.115970>
- Wei M, Kaneko Y, Shi P, Liu Y (2018) Numerical modeling of dynamically triggered shallow slow slip events in New Zealand by the 2016 M_w 7.8 Kaikōura earthquake. *Geophys Res Lett* 45:4764–4772. <https://doi.org/10.1029/2018GL077879>
- Wu YM, Chang CH, Zhao L, Teng TL, Nakamura M (2008) A comprehensive relocation of earthquakes in Taiwan from 1991 to 2005. *Bull Seis Soc Am* 98:1471–1481. <https://doi.org/10.1785/0120070166>
- Wu YM, Shyu JBH, Chang CH, Zhao L, Nakamura M, Hsu SK (2009) Improved seismic tomography offshore northeastern Taiwan: implications for subduction and collision processes between Taiwan and the southernmost Ryukyu. *Geophys J Int* 178:1042–1054. <https://doi.org/10.1111/j.1365-246X.2009.04180.x>
- Wu YM, Chen SK, Huang TC, Huang HH, Chao WA, Koulakov I (2018) Relationship between earthquake b-values and crustal stresses in a young orogenic belt. *Geophys Res Lett* 45:1832–1837. <https://doi.org/10.1002/2017GL076694>
- Xie S, Dixon TH, Malservisi R, Jiang Y, Protti M, Muller C (2020) Slow slip and inter-transient locking on the Nicoya megathrust in the late and early stages of an earthquake cycle. *J Geophys Res*. <https://doi.org/10.1029/2020JB020503>
- YabukiMatsu'ura TM (1992) Geodetic data inversion using a Bayesian information criterion for spatial distribution of fault slip. *Geophys J Int* 109:363–375. <https://doi.org/10.1111/j.1365-246X.1992.tb00102.x>

- Yokota Y, Ishikawa T, Watanabe S, Tashiro T, Asada A (2016) Seafloor geodetic constraints on interplate coupling of the Nankai Trough megathrust zone. *Nature* 534:374–377. <https://doi.org/10.1038/nature17632>

Publisher's Note

Springer Nature remains neutral with regard to jurisdictional claims in published maps and institutional affiliations.

Submit your manuscript to a SpringerOpen® journal and benefit from:

- Convenient online submission
- Rigorous peer review
- Open access: articles freely available online
- High visibility within the field
- Retaining the copyright to your article

Submit your next manuscript at ► [springeropen.com](https://www.springeropen.com)